Targeted pulmonary drug delivery in coronavirus disease (COVID-19) therapy: A patient-specific in silico study based on magnetic nanoparticles-coated microcarriers adhesion

Sina Ebrahimi, Amir Shamloo [*], Mojgan Alishiri, Yasaman Mozhdehbakhsh Mofrad [1], Fatemeh Akherati [1]

School of Mechanical Engineering, Sharif University of Technology, Tehran, Iran

ABSTRACT

Since the beginning of the COVID-19 pandemic, nearly most confirmed cases develop respiratory syndromes. Using targeted drug delivery by microcarriers is one of the most important noteworthy methods for delivering drugs to the involved bronchi. This study aims to investigate the performance of a drug delivery that applies microcarriers to each branch of the lung under the influence of a magnetic field. The results show that by changing the inlet velocity from constant to pulsatile, the drug delivery performance to the lungs increases by ~31%. For transferring the microcarriers to the right side branches (LUL and LLL), placing the magnet at zero height and ~30° angle yields the best outcome. Also, the microcarriers' delivery to branch LUL improves by placing the magnet at LUL-LLL bifurcation and the angle of ~30°. It was observed that dense ($9300[\frac{kg}{m^3}]$) microcarriers show the best performance for delivering drugs to LLL and RLL&RML branches. Also, low-density ($1000[\frac{kg}{m^3}]$) microcarriers are best for delivering drugs to LUL and RUL branches. The findings of this study can improve our understanding of different factors, such as inlet velocity, the magnet's position, and the choice of microcarrier – that affect drug delivery to the infected parts of the lung.

1. Introduction

Since the outbreak of the COVID-19 pandemic, around 216 million people have been infected with Coronavirus worldwide, and around 4.5 million have died because of it (https://covid19.who.int/ as of 30 August 2021). As of August 2020, according to Tzotzos et al. (2020) ~ 20%of the cases required hospitalization due to respiratory problems, and among the hospitalized patients who later died, Acute Respiratory Distress Syndrome (ARDS) and pneumonia were the leading causes (Hasan et al., 2020). ARDS is a condition that develops from pneumonitis or inflammation in different parts of the lungs. In COVID-19, inflammation occurs in the peripheral regions of the lungs where alveoli are located (Chung et al., 2020). Corticosteroids which are basically anti-inflammatory agents are widely used to treat this condition in the disease (Liu et al., 2020). However, there has been some studies suggesting that IL-6 agents and HCQ could also be beneficial to treat pneumonitis in COVID-19 (Kavanagh et al., 2020; Zhou and Price,

2020). Nevertheless, the ultimate drug of choice in the current study is the class of inhaled corticosteroids (ICS) since the applied method in this study is fundamentally based on inhalation. An ideal ICS should possess certain characteristics including pulmonary deposition efficiency, low oral bioavailability, high systemic clearance, optimized pulmonary residence time and selective binding to glucocorticoid receptor. In a targeted drug delivery system, almost all of these characteristics could be generalized to the delivery method. Since the present developed corticosteroids have checked the boxes of the mentioned characteristics to their fullest potential, it can be concluded that new developments should focus on delivery methods and devices to achieve the best results (Hochhaus, 2004).

Targeted drug delivery is a set of mechanisms that contribute to the aggregation of drugs in a specific part of the body (i.e. organ, tissue, cells) that has been affected by diseases. From a theoretical perspective, each drug delivery system has two principal goals: first, enhancing drug efficiency, and second, inhibiting drug penetration to healthy parts of

the body. Drug delivery process is completed using appropriate carriers for the drugs. Type, chemical compound, size, shape, morphology and the surface chemistry of these carriers directly affect their behavior, distribution, and therefore the targeted drug delivery process (Sun et al., 2008). Among other factors that affect the drug delivery process is inlet velocity magnitude of fluid and airflow pattern in the lungs (Sohrabi et al., 2014). Designing a proper targeted drug delivery system requires optimizing the response of various therapeutic carriers to external fields. Among these external fields, the magnetic field is the most commercially used since 1970, and it has a broad scope of application (Lübbe et al., 2001; Widder et al., 1978).

The type of drug carrier is vital, and it directly affects the distribution of the drug in the targeted site. In terms of toxicity, the main concern is that small-sized nanoparticles might cause injury and inflammation in the lung. It has been shown that small-sized nanoparticles are more likely react negatively to biological structures compared to large-size particles. However, most experiments have investigated this matter in vitro, and only a few in vivo studies have been carried out (Gill et al., 2007). Microbubbles (MBs) adhere to the injured areas of the endothelium, and they can be a suitable carrier for treating pulmonary injuries caused by COVID-19 and SARS (Sirsi et al., 2013). Due to their magnetic properties and their response to an external magnetic field, magnetic particles can also be utilized in drug delivery. Most of these particles are made of Fe_3O_4 (magnetite) or γ-Fe_2O_3, and they are coated with polymers. Because of the benefits of their unique properties, there are also carriers made from gold or silica. For instance, particles made from iron have a high magnetic quality, and coating them with gold or silica makes them more stable (Sun et al., 2008). If these particles are suitably coated, they would have a wide variety of use in medical applications such as drug delivery (Gupta et al., 2007). As for MBs containing superparamagnetic iron oxide nanoparticles (SPION), some experimental studies such as Barrefelt et al. (2013) and Chertok and Langer (2018) have shown that they display no signs of toxicity, and they are safe to apply. Furthermore, the biodistribution and pharmacokinetics of SPION have been evaluated, and it has been shown that magnetic MBs (SPION microbubbles) eventually distribute to the liver and spleen. Chertok and Langer (2018) have expressed that the majority of these particles distribute to the liver (68 ± 11% dose/g tissue) and another fraction to the spleen (19 ± 10% dose/g tissue). However, MBs do not retain in these organs and have a relatively low half-life. Barrefelt et al. (2013) have also observed SPION MBs in the same organs and tracked them until their elimination. They have also expressed that no signs of toxicity (i.e. necrosis, inflammation, and fibrosis) were observed in these organs. Therefore, the administration of SPION MBs does not give rise to toxicity and adverse effects in any way.

In targeted drug delivery for pulmonary diseases, mostly, inhaler drugs are used (Kannan et al., 2018). Type and size of drug carriers, air passage geometry, flow regime, and considering the ligand-receptor binding are all effective on the quality of the drug delivery (Saadat et al., 2020; Shamloo et al., 2020). Also, velocity magnitude and its time dependency affect particle deposition and adhesion. According to a previous study, particle aggregation in bifurcations increases in cases with time variable velocities (Sohrabi et al., 2014). Moreover, Most coarse particles deposit in the upper airways while many smaller particles pass the lower airways, and some of them even reach the alveoli (Islam et al., 2017). In terms of flow regime, the flow is laminar in all parts of the lung except for the upper airways (Islam et al., 2017).

A lot of in vivo and in vitro studies have surveyed the delivery biocompatibility and efficiency of drug carriers while using magnetic fields. Verma et al. (2013) have evaluated the biocompatibility of Fe_3O_4 magnetic nanoparticles containing quercetin and coated by PLGA by their effects on glutathione and IL6 secretion. Their results demonstrate that the mice in the experiment did not show any symptoms of pulmonary disorders. After culturing cancer cells in mice lungs (male c57bl/6 mice), Alvizo-Baez et al. (2016) injected chitosan-coated nanoparticles into mice tails and pulled the nanoparticles towards the lung by a

magnet placed above the mice rib casge. They observed that in addition to pulling nanoparticles into lungs, the magnetic field caused morphological changes in cells – that lead to the activation of some promoters and controlling the gene expression of TRAIL protein which eventually caused a considerable reduction in the number of pulmonary tumors. Surveying pulmonary drug delivery to mice using Triptolide-loaded liposomes, Lin et al. (2017) observed in the fluorescence images that liposomes were only seen in the lungs and resided there 96 h. Price et al. (2017) placed a ~0.58T cylindrical permanent magnet above the upper left side of a mouse's lungs (a male Balb/c mouse). The results of their study demonstrated that the left side of the lungs absorbed higher level of drugs in presence of a magnetic field than its absence. They concluded that because of structural characteristics of the lungs such as large surface, permeable membrane and long capillaries, it is possible that the drugs are locally absorbed, and targeted drug delivery along the imposition of a magnetic field leads to drug aggregation in the target site – which helps recovering the organ from the disease and reducing toxicity in healthy tissues. In their in vitro study aimed at evaluating targeted drug delivery using a magnetic field, Poh et al. (2019) applied a setup consisting of a hollow tube (simulating the lungs), a smart inhaler, an actuator and four permanent magnets adjacent to the tube. The particles were released from the smart inhaler to the tube controllably and in a pulsatile pattern, and the bottom of the tube was connected to a fume hood. Moreover, the magnets were placed in different positions of ~0, ~10, and ~20 millimeters from the tube. In all positions, the particles moved towards the magnets and deposited in their proximity. The results showed by an increase in the magnetic force to gravity ratio particle deposition rate increases.

Since a magnetic field can encourage drug concentration in places most needed and prevent drug penetration to healthy tissues – thus reducing side effects to the least, magnetic field utilization in targeted drug delivery is recognized as a unique approach (Ostrovski et al., 2021, 2016; Saadat et al., 2020). This approach is used for the treatment of a lot of pulmonary diseases and syndromes such as SARS, MERS, COVID-19, COPD, etc. The most important of all, utilizing magnetism has the advantage of being non-invasive to the body (Saadat et al., 2020). As it was mentioned earlier, due to certain limitations, experimental surveys focus on biocompatibility and efficiency of drug carrier delivery in animals with pulmonary injuries whereas Poh's in vitro study (Poh et al., 2019) showed the importance of magnet position effect on drug delivery rate. Therefore, surveying magnet position effect on the rate of drugs delivered to human lungs can generate more realistic results through a genuine modeling of human lungs with accurate dimension and geometry. Numerical modeling can be a robust means with the least limitations and costs in this field of study. In previous numerical studies (Faizal et al., 2020; Huang et al., 2021), drug carriers were only assumed solid particles, and no ligand-receptor binding were considered. As it was mentioned earlier, the type of drug carrier is very determining in drug delivery processes; thus, in order to accurately model a drug delivery system ligand-receptor binding should be included. Moreover, studying the effects of drug carrier type on drugs delivered to each branch of the lungs could be worth noticing which has never been evaluated in previous numerical and experimental studies. In addition, while magnet position with respect to the patient's body is crucial in drug delivery results and in the process itself, the distance between the magnet and the patient's chest has also never been determined in previous studies.

In the current study, delivering the microcarriers to the inner surface of the lungs is surveyed. The delivery is improved by imposing an external magnetic field, and its efficiency is measured based on the surface density of microcarriers adhered to the inner walls of lung via ligand-receptor binding. The air is considered a Newtonian fluid, and the airflow is considered laminar. To investigate the effects of air velocity on microcarrier's adhesion to the inner surfaces of each of the lung's branches, airflow is considered in two different states: constant velocity and pulsatile. The simulation is also conducted in a patient-specific

geometry. Moreover, a permanent magnet is also placed in different positions outside of the patient's body so that the magnet position effect on the delivery of the magnetic nanoparticles-coated microcarriers to the target surfaces could be investigated. The microcarrier's type on delivering them to target surfaces is also studied in this survey. Different types of microcarriers differ in their shell structures, which eventually, results in different densities. This case is studied with and without the presence of the magnetic field.

2. Methods and materials

2.1. Geometry reconstruction

In order to accurately study the fluid flow in the lungs and tracking the particles in different regions of it, CT scan images (DICOM format) of a 48-year-old male has been used. This image has been processed by MIMICs software and then exported to a CAD software (Biglari et al., 2019). Human lung has different branches called 'generations' (Patwa and Shah, 2015). Whenever the airway splits into two branches the number of the generation increases. In total, the lung has ~23generations, G_0 being trachea and G_{23} being the alveoli. There is also another interpretation of the structure of lungs. This interpretation categorizes lungs into five lobes: Left Lower Lobe (LLL), Left Upper Lobe (LUL), Right Upper Lobe (RUL), Right Lower Lobe (RLL), and Right Middle Lobe (RML). In our study, we have considered RLL and RML as a single lobe, and this way, the whole lungs will have four main lobes (branches) (Fig. 1). Moreover, for one of the steps of the study, a permanent magnet was implemented to investigate the effects of a magnetic field on the surface density of microcarriers adhered to the inner walls of lung. The permanent magnet was placed at a certain distance to the lungs, as can be seen in Fig. 2.

2.2. Fluid properties and boundary conditions

In this study, air is considered as a Newtonian fluid with a constant density and dynamic viscosity of $\sim 1.185 kg/m^3$ and $\sim 1.82 \times 10^{-5} Pa.s$, respectively (Sabz et al., 2019). Also, two cases of constant and variable velocity are dedicated to the inlet's boundary condition (Nilsestuen and Hargett, 2005; Ostrovski et al., 2019). Intermittent Mandatory Ventilation (IMV) is one of the ventilation modes that is used for coronavirus patients. In this study, IMV has been used to simulate the variable velocity as shown in Supplementary Fig. 1. Other ventilation modes can

also be used since this matter is patient-specific, and the medical professionals should decide the proper ventilation mode based on the patient's condition (Lepper and Muellenbach, 2020). The outlet boundary condition is constant pressure, and it is equal to zero – relative to the atmospheric pressure (Islam et al., 2017). For the maximum inlet velocity of air, the Reynolds number has been calculated and equal to ~2100; according to which the flow regime is laminar.

2.3. Magnetic field

Nowadays, the application of magnetic nanoparticles in drug delivery is attracting notice as a double therapeutic advantage (Hayashi et al., 2010; Liu et al., 2008). In addition to facilitating the drug carrier delivery to the target site, an external magnetic field can promote drug release via a temperature increase in the cell membrane when drugs reach their target. Induced heat emanated by magnetic nanoparticles in the presence of a high-frequency magnetic field causes a considerable temperature increase for a short period which eventually facilitates drug release (Liu et al., 2008). In such a process, the frequency and intensity of the appointed magnetic field are so effective on the generated heat stimulating drug release that the percentage of drug release can be controlled by regulating the governing parameters of the external magnetic field; so much so that surveys have shown arranging a low-frequency magnetic field can promote the acceleration of drug release (Fang et al., 2016; Urbina et al., 2008). In the study by Cai et al. (2015) regarding drug delivery, $CoFe_2O_4$ microspheres containing Doxorubicin Hydrochloride (DOX) were exposed to magnetic fields whose frequency and intensity ranged respectively 0–400 Hz and 3–9 A. Their results showed the strong response of $CoFe_2O_4$ microspheres to a changing magnetic field which demonstrates the magnificent capability of this kind of drug carrier in magnetic steerage and drug release. In this case, the intended drug was released to the target site at a higher rate than those in the other tissues. The level of released drug in the presence of a 200 Hz magnetic field was ~54.6%, whereas in the absence of a magnetic field, it was ~29.5%. Therefore, Cai et al. concluded that a magnetic field could significantly enhance drug release. An increase in the frequency and intensity of a magnetic field contributes to a higher drug release rate. Marín et al. (2018) compared the controlled release of Acetaminophen (APAP) using films of gelatin/magnetite nanoparticle composite and under the influence of magnetic fields caused by fixed magnets (NdFeB – grade 52 N) with magnetic field strengths of ~0.3 and ~0.5T at room temperature of ~23 °C and also in the absence of a
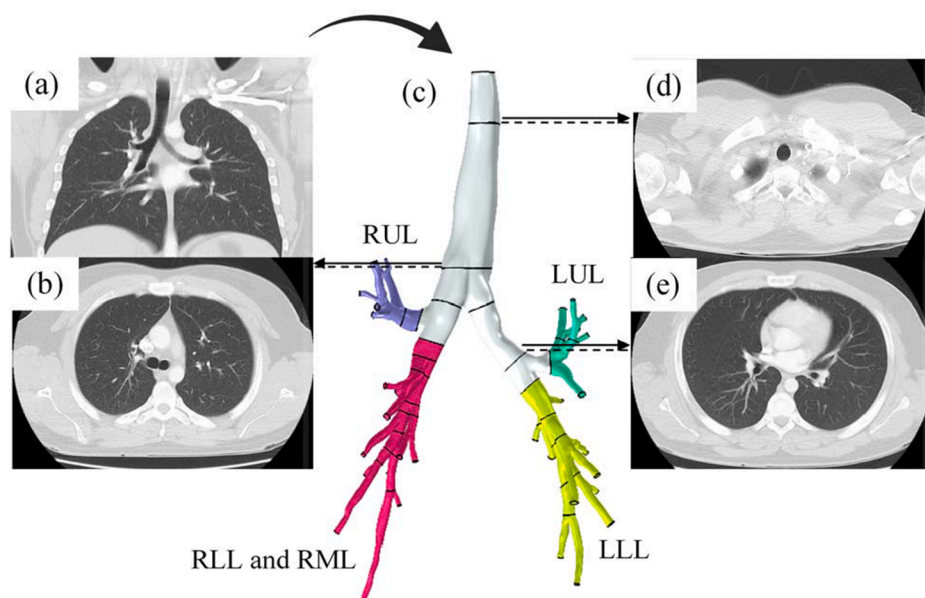

Fig. 1. CT scan images of the patient's lungs in two different cross-sections: (a) frontal plane b,d,e) transverse planes to distinguish between different branches of the lungs. C) extracting the 3D geometrical model from 2D CT images using an image processing software, generating the CAD model by excluding the excess branches, and finally, the segmentation of the lungs into four main lobes. Blue) Right Upper Lobe (RUL), green) Left Upper Lobe (LUL), red) Right Lower Lobe (RLL) and Right Middle Lobe (RML), and yellow) Left Lower Lobe (LLL).
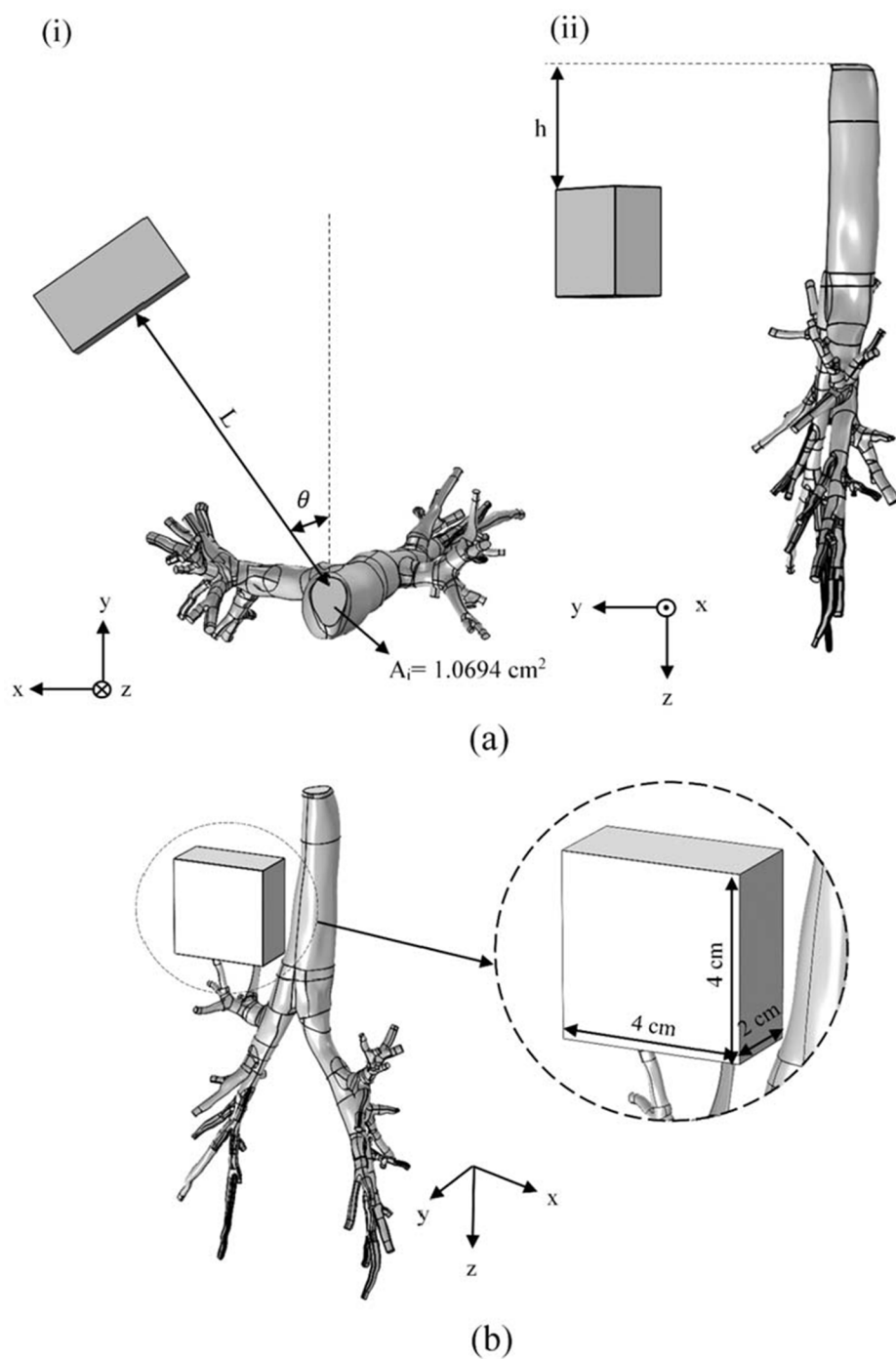
(i)

(ii)

Fig. 2. placing a permanent magnet attached to the patient's body in a way that NP-coated micro-carriers become affected through the magnetic field and deviate towards the target area so that it contributes to the enhancement of the drug delivery effectiveness. (a) the magnet is placed at three different heights, $h = 0cm$, $h = 25cm$, $h = 50cm$, concerning the lungs' inlet ($A_i = 1.0694cm^2$) and two different angles $\theta = 30°$ and $\theta = 60°$, in order to lead the microcarriers to the first bifurcation (LUL and LLL). The effect of the magnet's position angle on microcarriers' path in a case where the magnet was placed at the lungs' inlet ($h = 0cm$) is investigated. Moreover, the effect of a change in the magnet's height with respect to the lungs' inlet in the case where the magnet is placed at a constant $\sim30°$ angle is studied. In addition, the level of microcarriers' deviation from the target branches was investigated by placing the magnet in front of the bifurcation at two different angles of angles $\theta = 30°$ and $\theta = 60°$. The magnet's distance (L) from each of the target branches was also obtained from the CT scan images. Choosing the distance based on the human anatomical structure makes the results of the numerical solutions more realistic. (b) The dimension of the magnet is set $\sim4 \times 4 \times 2cm$ in all simulations. In order to model the closed lines of the magnetic field, a hollow box is considered to be around the magnet (the block is hidden in this figure).

magnetic field). They concluded that the percentage of drug release changes with the field magnitude.

In this study, A permanent magnet with a size of $\sim4 \times 4 \times 2cm$ was implemented. Moreover, we investigated the motion and migration of the magnetic nanoparticles (Fe_3O_4) coated microcarriers affected by a magnetic field. The diameter and magnetic susceptibility of magnetic nanoparticles were $\sim10nm$ and ~1.186, respectively. The saturation magnetization of these nanoparticles are $\sim448000A/m$ (Xu et al., 2005). The maximum magnitude of the external magnetic field (H_a) in the lung was estimated $\sim15320A/m$. Thus, based on Eq. S11, it is determined that Fe_3O_4 nanoparticles will not be magnetically saturated by the magnetic field produced by the implemented permanent magnet. Details of the magnetic field are given in Supplementary Note 1.

2.4. Forces

Forces exerted on the particles fall into two categories of external and interactive forces. External forces being gravity, Brownian, lift, drag, and the interactive forces being interaction forces between the particles. These are further explained in Supplementary Table 1. Since the flow regime is considered to be laminar, it is sufficient to only consider the first three terms of the drag coefficient. Also, the gravity force is directed towards the negative y-axis (Fig. 2.b) (Ebrahimi et al., 2021). In order to simulate the particle's interaction, Lennard-Jones potential is applied. This interaction is due to the Van der Waals force that attracts particles to each other, and the repulsive force resulted from electron cloud overlap. Lennard-Jones potential is usually chosen because of its

simplicity (Jorgensen and Tirado-Rives, 1988). There is also a magnetic force that is discussed and explained comprehensively in Supplementary Note 1. Forces imposed on the particles are schematically shown in Fig. 3.

The applied model in this study is the Lagrangian-Eulerian model. The air and microcarriers are considered continuous and discrete, and the Eulerian and Lagrangian frameworks are utilized corresponding to each, respectively (Forouzandehmehr and Shamloo, 2018; Shamloo and Forouzandehmehr, 2019; Tan et al., 2013). Through this method, the position and velocity of each particle with respect to time is extracted by solving for the second law of Newton (Amani et al., 2021; Shamloo et al., 2020). Also, one-way coupling is assumed since the fluid is air, having a low particle concentration - based on drug dosage distribution. The models in which the particle volume fraction is less than ~1% are referred to as dilute models (Umbarkar and Kleinstreuer, 2015).

2.5. Drug carrier adhesive dynamics model

In this study, we focus on micro-scale particles ($\sim 1 - 4 \mu m$ diameter) as drug carriers. Also, $20 nm$ difference due to magnetic nanoparticles diameter is somewhat negligible, and therefore, the magnetic MBs diameter is finally considered to be the same as the diameter of microcarriers. Optison is a suitable MB for this application (Shamloo et al., 2020). Physical properties of the microcarriers can be seen in Supplementary Table 2. The simulations were carried out in four seconds, and at the beginning of each second, ~1250 numbers of particles were released into the airway (Ostrovski et al., 2019).

Probability of particle adhesion to the walls is extracted and calculated by the ligand-receptor model (Nowak et al., 2003). The probability and intensity of adhesion depends on the surface molecules of the particles and the wall. Dislodge forces are affected by physiological factors such as wall shear stress and particle shape and size. Drag force (F) and
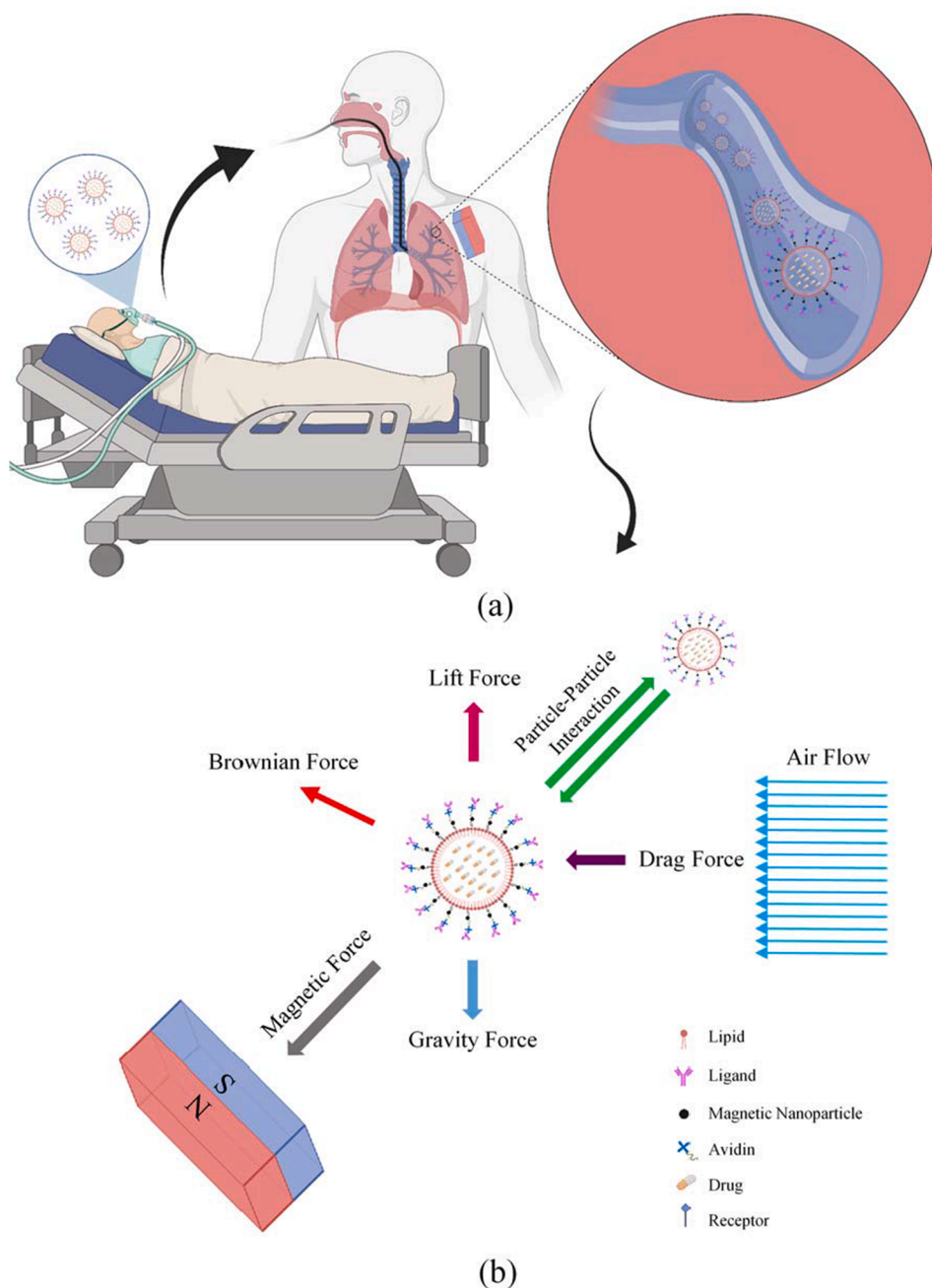

(a)

(b)

Fig. 3. Effective drug delivery to the lungs with the help of magnetic force among the patients suffering from respiratory syndromes is of the COVID-19 side effects. (a) to treat the remaining side effects in patients whose lungs have been affected by this disease, one of the therapies is done through targeted drug delivery. This treatment is initialized by loading the drugs into the microcarriers and the microcarriers entering the lungs by inhalation. Magnetic nanoparticles also coat the carriers. Adherence of the carriers to the receptors existing on the inner surface of the lungs' walls occurs through the ligands attached to the carrier's outer surface. Eventually, the drug reaches the target site more effectively, and the drug delivery process will be accomplished. (b) In addition to the magnetic force, other forces are also imposed on the microcarriers, which result from their presence in the airflow inside the lungs. The direction of the drag force (F_D) imposed on microcarriers is aligned with airflow and causes the microcarriers' forward motion. The lift force (F_L) caused by the air inside the lungs is imposed on the microcarriers in a direction perpendicular to that of the airflow and promotes the microcarriers' lateral motion. Due to the random collision of the microcarriers with other atoms or molecules, the Brownian force (F_B) is caused. Lennard-Jones potential facilitates the calculation of the interactions between microcarriers. Moreover, the imposition of the gravity force on the microcarriers is also considered.

torque (T) depend on the separation distance from the substrate (l), particle's diameter (d_P), and shear stress (μS).

$$F = 6\pi l \mu S F^S \tag{1}$$

$$T = 0.5\pi d_P^3 \mu S T^S \tag{2}$$

the coefficients F^S and T^S for spherical particles are 1.668 and 0.944, respectively.

Adhesion probability is also defined as:

$$P_a = m_r m_1 K_a^0 \pi r_0^2 \exp\left[-\frac{\lambda d_P \mu S}{2 k_B T r_0^2 m_r} \left[6\left(d_P/2 + \delta_{eq}\right)F^S + 2\frac{d_P^2}{r_0}T^S \right] \right] \tag{3}$$

in which m_r and m_1 are the receptor's and the legand's surface density, respectively. When particles are close enough to the target surface the ligand-receptor binding occurs. K_a^0 is association constant while the binding force is zero. Values of K_a^0 and m_1 depend on the particle type and chemical conditions (Sohrabi et al., 2014). δ_{eq} and $k_B T$ are the equilibrium separation distance between the particle and the substrate and thermal energy of Boltzmann, respectively. r_0 is the the radius of the interaction surface. The values of other parameters are given in Supplementary Table 3.

Based on our previous studies (Forouzandehmehr and Shamloo, 2018; Shamloo et al., 2020, 2019), governing partial differential equations in the simulations of the current study were solved with the assistance of a laboratory-made unsteady nonlinear finite element code. The equations regarding the physics of the laminar flow are transient and solved by the Algebraic Multigrid (AMG) algorithm using Backward Differentiation Formula (BDF) time solver featuring second degree accuracy and tolerance termination tech. Moreover, For tracking the particles, the generalized minimal residual (GMRES) solver was applied. For damped Newton iterations, a constant damping factor was utilized as a nonlinear method (Anderson, 1965; Curtiss and Hirschfelder, 2006; Dhamacharoen, 2016; Manzoori et al., n.d.; Toth et al., 2015). For obtaining the surface density of particles adhered to the inner wall of the lung, a certain variable was dedicated to each element of the lung airways. This variable was affected by every particle attached to the boundary element. Every time a particle is attached to the boundary element, the variable's value – which was initially set to ~1 by the source term – increased. Afterward, the source term was divided by the area of the boundary element.

In order to discretize magnetic field components in this study, second-order elements have been applied. For surveying the accuracy level of different discretization methods, three different methods of linear (first-order elements), quadratic (second-order elements), and cubic (third-order elements) have been used so that the amount of magnetic flux density in ~2cm proximity of the magnet is determined, and then, compared to that of analytical solution. In Supplementary Table 4, the obtained values of magnetic flux density from the simulations are gathered.

The magnetic flux density value surrounding the magnet is calculated through the analytical relation down below (Camacho and Sosa, 2013):

$$B(y) = \frac{\mu_0 M}{\pi}\left[\arctan\frac{ab}{(z-c)\sqrt{a^2+b^2+(z-c)^2}} - \arctan\frac{ab}{(z+c)\sqrt{a^2+b^2+(z+c)^2}} \right] \tag{4}$$

In the above expression, $\mu_0 M = 1.5(T)$, and a, b and c relate to the magnet's dimensions, which according to the applied magnet in this study, are ~2, ~2, and ~1cm. Z is the distance from the magnet, which corresponds to ~3cm in this study. The amount of magnetic flux density in the distance of ~2cm from the magnet was extracted analytically to be ~0.1158T. A noticeable discrepancy between the results of the simulations and those of theoretical solutions concerning magnetic flux

density were observed in first-order elements (~5.01%) rather than second-order elements (~0.69%) and third-order elements (~0.78%). This is an acceptable outcome since higher-order-element estimations are more accurate than lower-order-element ones. In addition to the results of second-order elements being more close to the analytical solution than third-order elements, the time required for third-order elements to solve is longer. Thus, second-order elements are a suitable choice to solve for the magnetic field.

In this targeted drug delivery system, the drugs are encapsulated in magnetic nanoparticles coated microcarriers and inhaled into the respiratory system. Then, through the pulmonary flow, the microcarriers reach the inflammation sites. The external force which can cause transverse movement in the motion of microcarriers is the magnetic force. The magnetic force directs the microcarriers toward the target site through the magnetic nanoparticles on their surface. Moreover, ligands on the surface of the microcarriers promote their adhesion to the target wall. They efficiently guide microcarriers to the target site through an external force, and cause small-dose drug transfer to the airways downstream the pulmonary flow.

3. Results and discussions

3.1. Particle transports and effect of inlet velocity on microcarrier adhesion

One of the effective parameters in microcarrier motion is the inlet velocity of air. Investigating this parameter could also be important in microcarriers' transfer and their adhesion to the inner surface of each branch. In this section, we study the effects of some parameters on the microcarrier adhesion to the inner walls. First, a schematic view of the particles' situation will be presented at different times. Second, the effects of flow velocity magnitude and its type (in terms of constant or pulsatile) on microcarrier adhesion to the inner surface of each branch will be investigated.

Deposition map for colored MBs based on their velocity magnitude for three states, ~1μm-diameter MBs with and without ligand and ~4μm-diameter MBs with ligand at multiple times is shown in the Supplementary Fig. 2. It can be seen that in $t = 0.5 s$ some MBs with ~4μm diameter have not reached the secondary airways while all of ~1μm-diameter MBs have reached the them at this time. This is explained by the fact that the particles' mass directly influences their motion (Eq. (3)). With comparison between the density of the ~1μm-diameter MBs with ligands in the last second ($t = 4s$) and that of without ligand, it can be seen that the MBs with ligands have higher density in bifurcations. This phenomenon implies the importance of the ligand-receptor binding in the adhesion of MBs to the walls of target branches.

In the current study, four velocities of ~0.05m/s, ~0.345m/s, ~0.574m/s, ~0.69m/s were used for investigating the effect of inlet velocity magnitude on the adhesion of the MBs. Fig. 4a shows the surface density of MBs adhered to the inner walls of each four main branches at each constant inlet velocity. According to this figure, it can be seen that by velocity decrease, the surface density of MBs adhered to the LLL and RLL&RML branches also considerably decreases. Although the surface density of MBs adhered to the branches LUL and RUL does not have a specific trend, it reaches its maximum value with ~0.574m/s velocity. Sohrabi et al. (2014) have observed in their numerical study that the increase in the inlet velocity does not cause an increase in the surface density of the ligand-coated particles adhered to the whole inner walls. This phenomenon is also observed in the current study and validates the results of particle simulations inside the lung. Fig. 4b shows the surface density of MBs adhered to the inner wall of branches for two states of constant (~0.345m/s) and pulsatile (with a mean of ~0.345m/s) inlet velocity. It is shown that a shift in the inlet airflow pattern from constant to pulsatile causes an increase in the surface density of MBs adhered to the whole walls. Considering all branches of the lungs, the surface
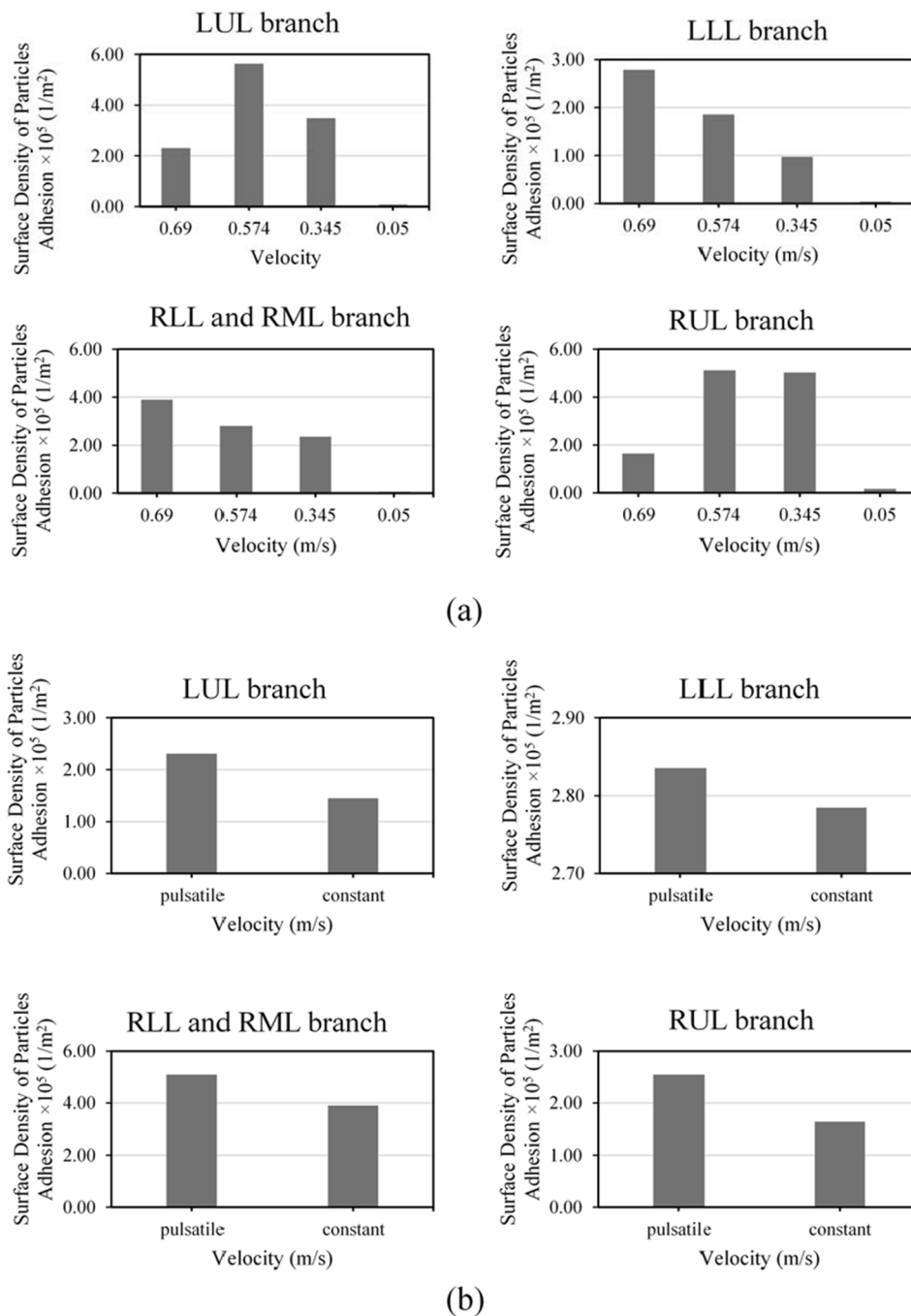
Fig. 4. (a) studying the effects of different inlet velocities, and (b) comparing the effects of constant inlet velocities of ~0.354m/s and pulsatile velocity with the average amount of ~0.345m/s on the surface density of MBs adhered to the inner walls of LUL, LLL, RLL and RML, and RUL branches.

density of MBs adhered to the walls in case of constant inlet airflow is ~9.77 × 10^5, and in the case of pulsatile inlet airflow, it is ~12.8 × 10^5. Therefore, when the inlet airflow pattern shifts from constant to pulsatile, the surface density of MBs adhered to the whole walls increases by ~31%. This effect is depicted in Supplementary Fig. 3 which shows the Average Particle Residence Time in all branches of the lung for both two cases of constant and pulsatile inlet airflow. The figure also shows ~32% increase in average MB residence time when the flow is pulsatile rather than constant. The higher the MBs residence time, the more probable it is for the particles to adhere to the walls, as shown in Fig. 4b.

### 3.2. Effect of magnetic field on delivery of microcarriers

Using magnetic force resulting from the magnetic field could be an effective strategy for making the drug delivered to the inflamed parts, especially for COVID-19 treatment. Although many numerical surveys (Saadat et al., 2020) concerning particle transfer towards a target site using a magnetic field have been carried out, their authors have used point magnetic fields, or they have considered the position of the magnet far too close to the lung - which is neither realistic nor applicable. Also, in the previous studies, there were no use of the ligand-receptor binding alongside the use of a magnetic field, which could be a practical option (Saadat et al., 2020). Investigating the drug delivery performance using the magnetic nanoparticles-coated ligand-attached microcarriers can

clinically improve our understanding of the effect of the magnet's position on the whole process of drug delivery to target branches. In order to study the performance of the microcarrier delivery to the right-side branches (LUL and LLL), the magnet was placed in different positions, and the amount of surface density of microcarriers adhered to the inner walls was obtained. Fig. 5a shows the amount of the surface density of MBs adhered to the inner walls for delivering MBs to the right-side branches in different magnet positions. It is observed that the adhesion increase of MBs affected by a magnetic field produced by a magnet placed at zero height and orientation angle of ~30° was ~19.5% and ~37.6% more than the case without the presence of the magnetic field for LUL and LLL branches, respectively. The negative influence of the magnet in delivering MBs to LUL and LLL branches is also observed by placing the magnet at zero height and orientation angle of ~60°. It is observed that although an increase in the magnet's height to ~ 25*mm* and ~50*mm* (becoming closer to the branches) causes an increase in the amount of surface density of MBs adhered to branch LUL by ~7.7% and ~2.9%, respectively, and to branch LLL by ~17.0% and ~8.83%,
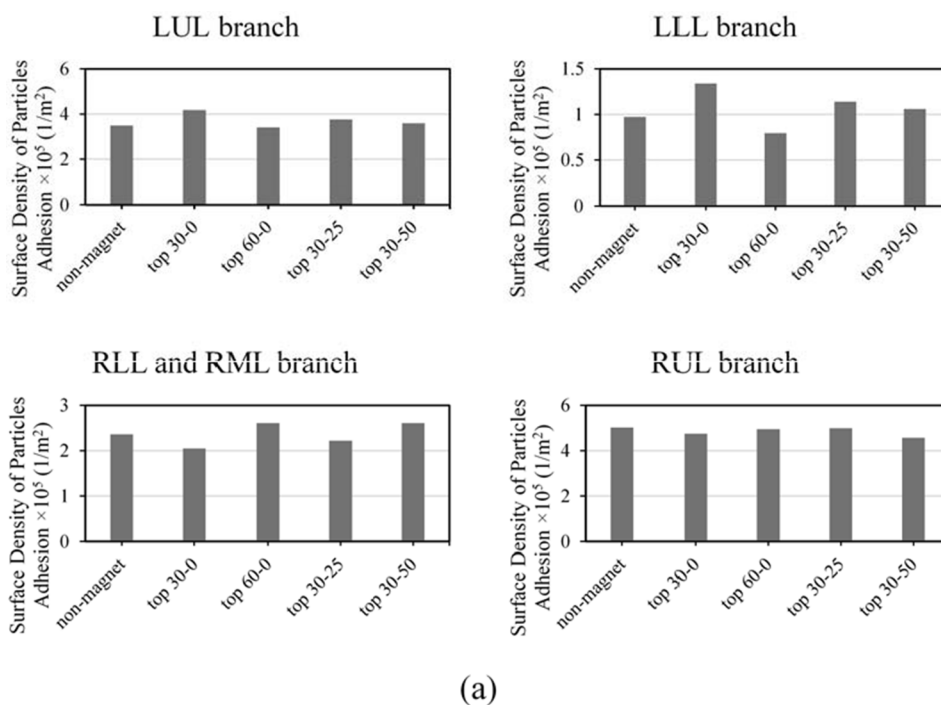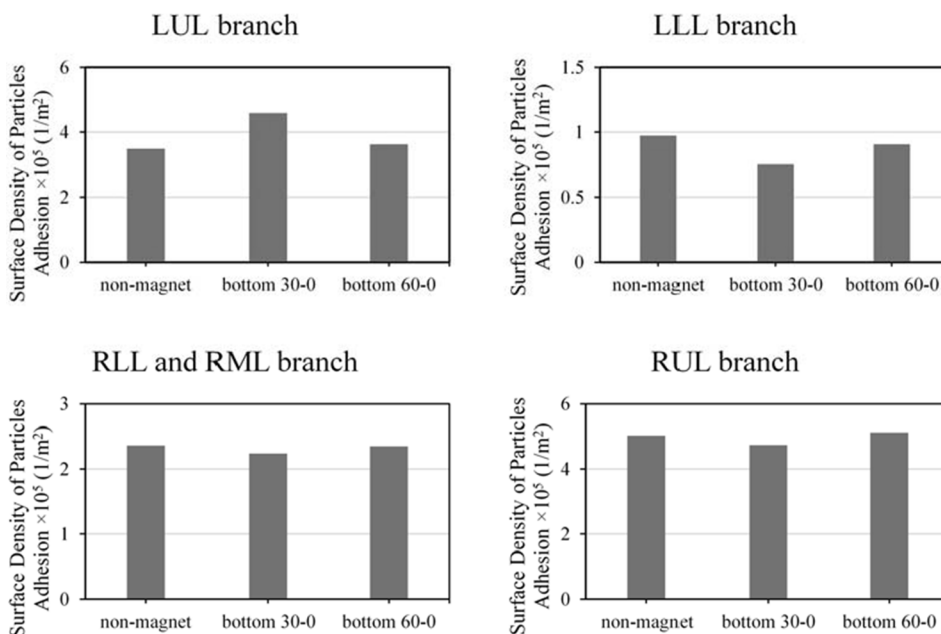
Fig. 5. Comparing the surface density of MBs (*diameter* $= 2\mu m$) adhered to the inner walls of LUL, LLL, RLL and RML, and RUL branches in the presence and without the presence of the magnetic field with the magnet's position set at (a) $h = 0cm$ and two different angles of $\theta = 30°$ and $\theta = 60°$, and at angle $\theta = 30°$ and two different heights of $h = 25cm$ and $h = 50cm$ (b) the bifurcation at two angles of $\theta = 30°$ and $\theta = 60°$.

respectively, it contributes to lower efficacy compared to the position in which the magnet is at zero height (close to the neck). With regards to the results, it is observed that placing the magnet at zero height (close to the neck) in ~30° angle contributes to the highest performance of MB delivery to the target branches LUL and LLL. This phenomenon could have been caused by the high magnitude of magnetic field and its direction at the mentioned position concerning the other magnet positions (Supplementary Fig. 4).

By comparing the magnet's effect using the best position for LUL and LLL branches (zero height, angle of ~30°), the MB delivery level to branch LLL is higher than to branch LUL. The microcarriers were pushed towards branch LUL by placing the magnet at LUL-LLL bifurcation. Hence, we placed a magnet at LUL-LLL bifurcation at two angles of ~30° and ~60° Fig. 5b shows the surface density of MBs adhered to the inner walls of the lungs for two angles of ~30° and ~60°. It was observed that by placing the magnet at the angle of ~30° for delivering to the target branch LUL, the amount of the surface density of MBs adhered to the inner walls of target branch LUL increases by ~31.5% than that without the presence of the magnetic field. While for the magnet position in which it is placed at ~60° angle, this enhancement is only ~4.1% - which is meager. This phenomenon happens due to the considerable decrease in the magnitude of the magnetic field at the angle of ~60°which is discussed further in Supplementary Note 4. It can be said that compared to the position close to the neck, in which the magnet is at zero height, placing the magnet at LUL-LLL bifurcation and angle of ~30° contributes to a far better performance in delivering drugs to branch LUL.

The simulation results show that by placing the magnet at the angle of ~30° and ~60°, the amount of the surface density of MBs adhered to the inner walls of LLL, RLL, RML and RUL than the decreases compared to the absence of the magnetic field. The cause of this phenomenon is the higher transfer rate of MBs entering the lung and moving towards the LUL branch under the influence of the magnetic field. It also decreases the number of MBs migrating towards the other branches and causes the adhesion to other branches (LLL, RLL, RML, and RUL) to decrease – in the presence of the magnetic field in the situation mentioned above.

The clinical and experimental surveys show the importance of toxicity and dose control of pulmonary drugs by studying the absorption level of inhaled microcarriers containing drugs through the lung's inner walls. Therefore, surveying the amount of drug absorption in the presence and absence of a magnetic field can improve our understanding towards the effect of a magnet's presence and its position on the absorption of drug carriers inhaled into the lungs. The effect of the magnetic field's presence and absence on the surface density of microcarriers ($diameter = 2\mu m$) adhered to whole inner walls of the lung are shown in Fig. 6., in cases where the fixed magnet is placed at $h = 0$ cm and $\theta = 30°$ (Fig. 6a), and at LUL-LLL bifurcation in 30° angle (Fig. 6b). It is observed that the presence of a magnet contributes to an increase in the surface density of MBs adhered to the whole inner walls of the lung in a way that a magnet position corresponding to $h = 0$ cm and $\theta = 30°$ causes an increase of ~18%. Moreover, in a magnet position placed $\theta = 30°$ to the LUL-LLL bifurcation, the surface density of MBs adhered to the whole inner wall is increased by ~12%. This increase could be the cause of MBs attraction towards the walls and the cause of decrease in MB velocity due to the magnetic force overcoming drag forces caused by the airflow inside the lung. An increase in the surface density of MBs in the presence of a magnetic field causes an increase in their absorption to the walls and prevents further MB migration to farther sub-branches – which is an affecting factor in toxicity.

3.3. Effect of properties of microcarriers on their delivery

The microcarrier shell can be composed of inorganic material, affecting their density and stability during drug delivery (Huang et al., 2011; Liong et al., 2008; Tom et al., 2004). A change in microcarrier density directly affects the magnitude of gravity force and forces
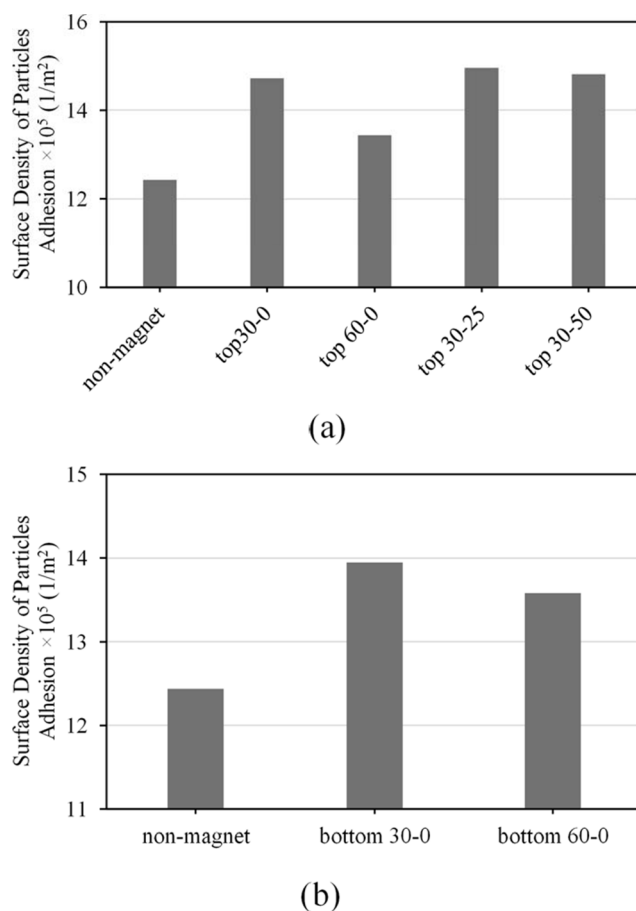

Fig. 6. Comparing the surface density of MBs ($diameter = 2\mu m$) adhered to the whole inner walls of lung in the presence and without the presence of the magnetic field with the magnet's position set at (a) $h = 0cm$ and two different angles of $\theta = 30°$ and $\theta = 60°$, and at angle $\theta = 30°$ and two different heights of $h = 25cm$ and $h = 50cm$ (b) the bifurcation at two angles of $\theta = 30°$ and $\theta = 60°$.

imposed by the surrounding fluid - namely, drag and lift forces. This factor can make a change in microcarrier motion inside the lungs. Previous studies on targeted drug delivery for arterial disease and cancer have shown the significance of microcarrier density on delivering drugs to target surfaces (Amani et al., 2021; Ta et al., 2018; Toy et al., 2011). However, the effect of microcarrier density on its adhesion to the inner walls of the lung has not yet been studied. The effect of a magnetic field on each of the microcarriers with different shell properties inside the lung has not been studied as well. Investigating these effects on delivering drugs to the lung can improve our insight into the choice of microcarriers.

By releasing ~$2\mu m$ diameter microcarriers into the lungs – which possess ligand bonds and are different from each other in terms of density (Silica dioxide:$2650[\frac{kg}{m^3}]$, Iron oxide:$5170[\frac{kg}{m^3}]$, Nickel dioxide:$6670[\frac{kg}{m^3}]$, and Gold: $9300[\frac{kg}{m^3}]$), we have studied the surface density of those adhered to the inner walls of lung branches, with and without the presence of the magnetic field. Fig. 7a shows the surface density of microcarriers with different densities adhered to the inner branch walls, in two states in which the magnetic field is present and in the other is not. If the magnetic field exists, the magnet is placed at zero height and orientation angle of ~30°. It should also be noted that the target branches of these microcarriers are LUL and LLL. In the case where no magnet is present, it is observed that an increase in microcarrier density causes a considerable decrease in the surface density of microcarriers adhered to LUL and RUL branches whereas the opposite occurs for LLL
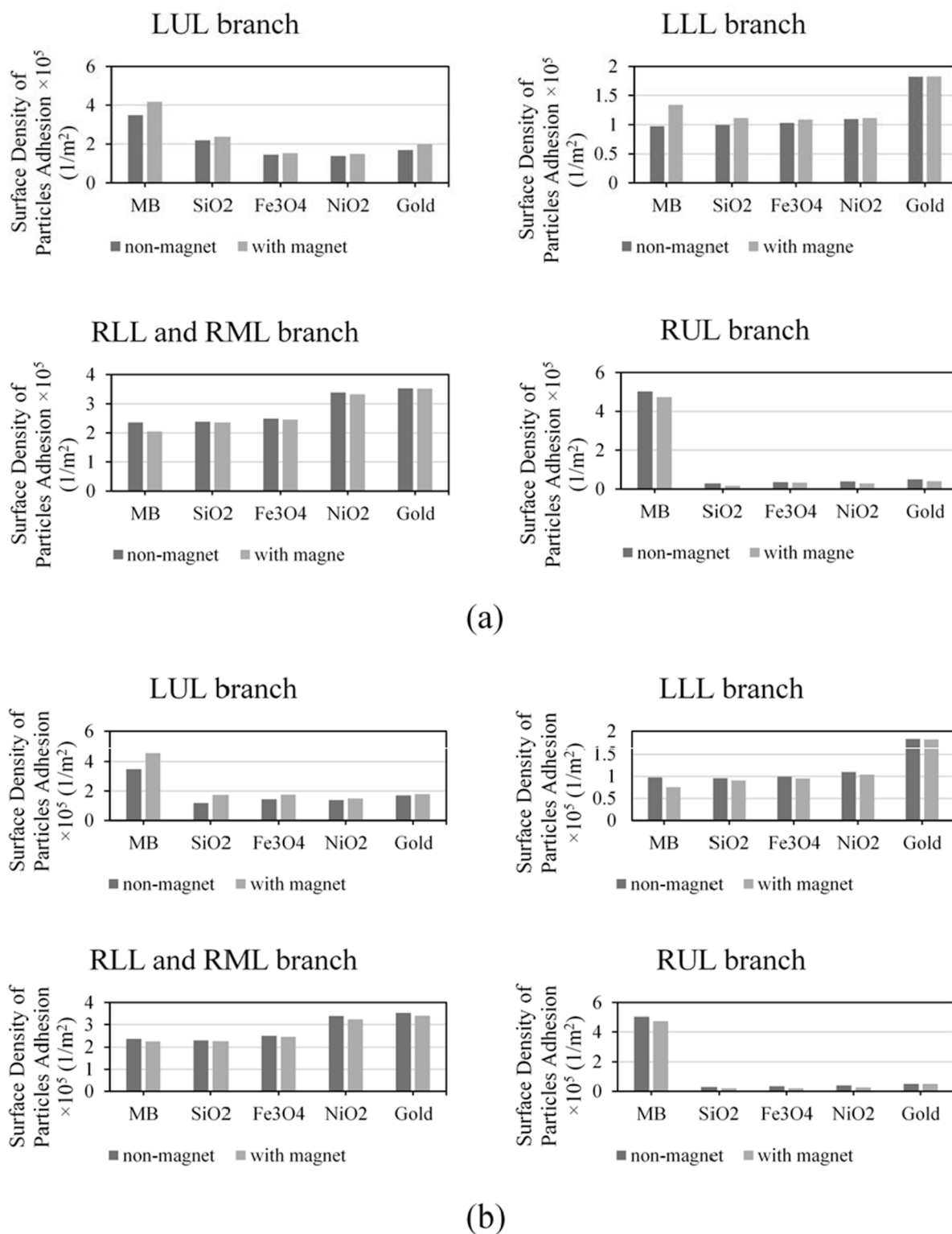
Fig. 7. The effect of the magnetic field's presence where the fixed magnet is placed (a) at $h = 0$ cm and $\theta = 30°$, and (b) at LUL-LLL bifurcation with an orientation angle of 30°, in comparison to its absence on the surface density of different microcarriers (*diameter* $= 2\mu m$) adhered to the inner walls of LUL, LLL, RLL and RML, and RUL branches.

and RLL&RML branches. As it was previously mentioned, appointing a magnetic field affects microcarrier path towards the target branches (LUL and LLL) whereas increasing microarrier density attenuates such an effect. This is also seen when the target branch is LUL, and the magnet is placed at LUL-LLL bifurcation in ~30°angle, (Fig. 7b). The reason for this phenomenon is that the higher the density of microcarriers, the

more the magnitude of the imposed forces are (Supplementary Table 1). Hoever, since the force resulting from the magnetic field is independent from the microcarriers density, its magnitude remains the same as before (Eq. S8). The presence of the magnetic field stabilizes the microcarriers in their path and decreases their deflection at high densities. Therefore, it can be concluded that the performance of the

magnetic field in the delivery process becomes higher for low-density microcarriers. It is notcible that the same behavior has been observed with microcarrier diameters of ~1, ~3, and ~4μm in the results of the simulations.

4. Conclusion

In our previous studies, we recruited computational techniques for modeling some biological phenomena (Ebrahimi et al., 2021; Forouzandehmehr & Shamloo, 2018; Shamloo et al., 2015, 2018; Shamloo et al., 2015, 2016, 2017). In this study, we investigated targeted pulmonary drug delivery using magnetic nanoparticles-coated microcarriers. We have shown that an increase in the inlet velocity magnitude causes an increase in the microcarrier adhesion to LLL and RLL&RML branches. Nonetheless, for LUL and RUL branches, an inlet velocity of ~0.574m/s yields the maximum adhesion. It was observed that changing the inlet velocity from constant to pulsatile can considerably enhance the drug delivery performance to the lungs. The results showed that for transferring the microcarriers to the right side branches (LUL and LLL), placing the magnet at zero height and ~30° angle yields the best outcome. Also, by placing the magnet at LUL-LLL bifurcation and angle of ~30°, the microcarriers delivery to branch LUL improves. By applying different microcarrier densities, either with and without the presence of a magnetic field, it was observed that dense microcarriers show the best performance for delivering drugs to LLL and RLL&RML branches. Also, low-density microcarriers are best for delivering drugs to LUL and RUL branches. Moreover, it was shown that increasing the density of the magnetic nanoparticles-coated microcarriers prevents their deviation towards target branches and causes a slump in magnetic field effect on drug delivery performance.

CRediT authorship contribution statement

Sina Ebrahimi: Conceptualization, Data curation, Formal analysis, Investigation, Methodology, Software, Validation, Visualization, Writing – original draft, Writing – review & editing. **Amir Shamloo:** Conceptualization, Formal analysis, Investigation, Methodology, Project administration, Software, Supervision, Writing – original draft, Writing – review & editing. **Mojgan Alishiri:** Data curation, Formal analysis, Methodology, Software, Validation, Writing – original draft, Writing – review & editing. **Yasaman Mozhdehbakhsh Mofrad:** Data curation, Formal analysis, Methodology, Software, Writing – original draft, Writing – review & editing. **Fatemeh Akherati:** Data curation, Methodology, Software, Writing – original draft.

Declaration of Competing Interest

The authors declare that they have no known competing financial interests or personal relationships that could have appeared to influence the work reported in this paper.

Appendix A. Supplementary material

Supplementary data to this article can be found online at https://doi.org/10.1016/j.ijpharm.2021.121133.

References

Alvizo-Baez, C.A., Luna-Cruz, I.E., Vilches-Cisneros, N., Rodríguez-Padilla, C., Alcocer-González, J.M., 2016. Systemic delivery and activation of the TRAIL gene in lungs, with magnetic nanoparticles of chitosan controlled by an external magnetic field. Int. J. Nanomed. 11 https://doi.org/10.2147/IJN.S118343.

Amani, A., Shamloo, A., Barzegar, S., Forouzandehmehr, M., 2021. Effect of material and population on the delivery of nanoparticles to an atherosclerotic plaque: a patient-specific in silico study. Langmuir. https://doi.org/10.1021/acs.langmuir.0c03158.

Anderson, D.G., 1965. Iterative procedures for nonlinear integral equations. J. ACM 12 (4), 547–560. https://doi.org/10.1145/321296.321305.

Barrefelt, Å., Saghafian, M., Kuiper, R., Ye, F., Egri, G., Klickermann, M., Brismar, T.B., Aspelin, P., Muhammed, M., Dähne, L., Hassan, M., 2013. Biodistribution, kinetics, and biological fate of SPION microbubbles in the rat. Int. J. Nanomed. 8 https://doi.org/10.2147/IJN.S49948.

Biglari, H., Razaghi, R., Ebrahimi, S., Karimi, A., 2019. A computational dynamic finite element simulation of the thoracic vertebrae under blunt loading: spinal cord injury. J. Brazilian Soc. Mech. Sci. Eng. 41, 84. https://doi.org/10.1007/s40430-019-1588-z.

Cai, B., Zhao, M., Ma, Y.e., Ye, Z., Huang, J., 2015. Bioinspired formation of 3D hierarchical CoFe2O4 porous microspheres for magnetic-controlled drug release. ACS Appl. Mater. Interfaces 7 (2), 1327–1333. https://doi.org/10.1021/am507689a.

Camacho, J.M., Sosa, V., 2013. Alternative method to calculate the magnetic field of permanent magnets with azimuthal symmetry. Rev. Mex. Fis. E 59.

Chertok, B., Langer, R., 2018. Circulating magnetic microbubbles for localized real-time control of drug delivery by ultrasonography-guided magnetic targeting and ultrasound. Theranostics 8 (2), 341–357. https://doi.org/10.7150/thno.20781.

Chung, M., Bernheim, A., Mei, X., Zhang, N., Huang, M., Zeng, X., Cui, J., Xu, W., Yang, Y., Fayad, Z.A., Jacobi, A., Li, K., Li, S., Shan, H., 2020. CT imaging features of 2019 novel coronavirus (2019-NCoV). Radiology 295 (1), 202–207. https://doi.org/10.1148/radiol.2020200230.

Curtiss, C.F., Hirschfelder, J.O., 2006. Integration of stiff equations. Proc. Natl. Acad. Sci. https://doi.org/10.1073/pnas.38.3.235.

Dhamacharoen, A., 2016. Efficient numerical methods for solving differential algebraic equations. J. Appl. Math. Phys. 04 (01), 39–47. https://doi.org/10.4236/jamp.2016.41007.

Ebrahimi, S., Vatani, P., Amani, A., Shamloo, A., 2021. Drug delivery performance of nanocarriers based on adhesion and interaction for abdominal aortic aneurysm treatment. Int. J. Pharm. 594, 120153. https://doi.org/10.1016/j.ijpharm.2020.120153.

Faizal, W.M., Ghazali, N.N.N., Khor, C.Y., Badruddin, I.A., Zainon, M.Z., Yazid, A.A., Ibrahim, N.B., Razi, R.M., 2020. Computational fluid dynamics modelling of human upper airway: a review. Comput. Methods Programs Biomed. 196, 105627. https://doi.org/10.1016/j.cmpb.2020.105627.

Fang, J., Yang, Y., Xiao, W., Zheng, B., Lv, Y.-B., Liu, X.-L., Ding, J., 2016. Extremely low frequency alternating magnetic field-triggered and MRI-traced drug delivery by optimized magnetic zeolitic imidazolate framework-90 nanoparticles. Nanoscale 8 (6), 3259–3263. https://doi.org/10.1039/C5NR08086J.

Forouzandehmehr, M., Shamloo, A., 2018. Margination and adhesion of micro- and nanoparticles in the coronary circulation: a step towards optimised drug carrier design. Biomech. Model. Mechanobiol. 17 (1), 205–221. https://doi.org/10.1007/s10237-017-0955-x.

Gill, S., Löbenberg, R., Ku, T., Azarmi, S., Roa, W., Prenner, E.J., 2007. Nanoparticles: characteristics, mechanisms of action, and toxicity in pulmonary drug delivery - A review. J. Biomed. Nanotechnol. 3 (2), 107–119. https://doi.org/10.1166/jbn.2007.015.

Gupta, A.K., Naregalkar, R.R., Vaidya, V.D., Gupta, M., 2007. Recent advances on surface engineering of magnetic iron oxide nanoparticles and their biomedical applications. Nanomedicine 2 (1), 23–39. https://doi.org/10.2217/17435889.2.1.23.

Hasan, S.S., Capstick, T., Ahmed, R., Kow, C.S., Mazhar, F., Merchant, H.a., Zaidi, S.T.R., 2020. Mortality in COVID-19 patients with acute respiratory distress syndrome and corticosteroids use: a systematic review and meta-analysis. Expert Rev. Respir. Med. 14 (11), 1149–1163. https://doi.org/10.1080/17476348.2020.1804365.

Hayashi, K., Ono, K., Suzuki, H., Sawada, M., Moriya, M., Sakamoto, W., Yogo, T., 2010. High-frequency, magnetic-field-responsive drug release from magnetic nanoparticle/organic hybrid based on hyperthermic effect. ACS Appl. Mater. Interfaces 2 (7), 1903–1911. https://doi.org/10.1021/am100237p.

Hochhaus, G., 2004. New developments in corticosteroids. Proc. Am. Thorac. Soc. 1 (3), 269–274. https://doi.org/10.1513/pats.200402-007MS.

Huang, F., Zhu, Q., Zhou, X., Gou, D., Yu, J., Li, R., Tong, Z., Yang, R., 2021. Role of CFD based in silico modelling in establishing an in vitro-in vivo correlation of aerosol deposition in the respiratory tract. Adv. Drug Deliv. Rev. 170, 369–385. https://doi.org/10.1016/j.addr.2020.09.007.

Huang, H.C., Barua, S., Sharma, G., Dey, S.K., Rege, K., 2011. Inorganic nanoparticles for cancer imaging and therapy. J. Control. Release. https://doi.org/10.1016/j.jconrel.2011.06.004.

Islam, M.S., Saha, S.C., Sauret, E., Gemci, T., Gu, Y.T., 2017. Pulmonary aerosol transport and deposition analysis in upper 17 generations of the human respiratory tract. J. Aerosol Sci. 108, 29–43. https://doi.org/10.1016/j.jaerosci.2017.03.004.

Jorgensen, W.L., Tirado-Rives, J., 1988. The OPLS [optimized potentials for liquid simulations] potential functions for proteins, energy minimizations for crystals of cyclic peptides and crambin. J. Am. Chem. Soc. 110 (6), 1657–1666.

Kannan, R.R., Singh, N., Przekwas, A., 2018. A compartment–quasi-3D multiscale approach for drug absorption, transport, and retention in the human lungs. Int. J. Numer. Method. Biomed. Eng. 34 (5), e2955. https://doi.org/10.1002/cnm.v34.510.1002/cnm.2955.

Kavanagh, O., Marie Healy, A., Dayton, F., Robinson, S., O'Reilly, N.J., Mahoney, B., Arthur, A., Walker, G., Farragher, J.P., 2020. Inhaled hydroxychloroquine to improve efficacy and reduce harm in the treatment of COVID-19. Med. Hypotheses. 143, 110110. https://doi.org/10.1016/j.mehy.2020.110110.

Lepper, P.M., Muellenbach, R.M., 2020. Mechanical ventilation in early COVID-19 ARDS. EClinicalMedicine 28, 100616. https://doi.org/10.1016/j.eclinm.2020.100616.

Lin, C., Wong, B.C.K., Chen, H., Bian, Z., Zhang, G.e., Zhang, X., Kashif Riaz, M., Tyagi, D., Lin, G.e., Zhang, Y., Wang, J., Lu, A., Yang, Z., 2017. Pulmonary delivery of triptolide-loaded liposomes decorated with anti-carbonic anhydrase IX antibody

for lung cancer therapy. Sci. Rep. 7 (1) https://doi.org/10.1038/s41598-017-00957-4.

Liong, M., Lu, J., Kovochich, M., Xia, T., Ruehm, S.G., Nel, A.E., Tamanoi, F., Zink, J.I., 2008. Multifunctional inorganic nanoparticles for imaging, targeting, and drug delivery. ACS Nano 2 (5), 889–896. https://doi.org/10.1021/nn800072t.

Liu, F., Ji, C., Luo, J., Wu, W., Zhang, J., Zhong, Z., Lankford, S., Huang, H., Lin, F., Wang, Y., Mo, G., Hu, X., Jiang, T., Shao, Y., Ji, S., Zhang, Y., Qin, E., Mu, J., 2020. Clinical characteristics and corticosteroids application of different clinical types in patients with corona virus disease 2019. Sci. Rep. 10 (1) https://doi.org/10.1038/s41598-020-70387-2.

Liu, T.-Y., Hu, S.-H., Liu, K.-H., Shaiu, R.-S., Liu, D.-M., Chen, S.-Y., 2008. Instantaneous drug delivery of magnetic/thermally sensitive nanospheres by a high-frequency magnetic field. Langmuir 24 (23), 13306–13311. https://doi.org/10.1021/la801451v.

Lübbe, A.S., Alexiou, C., Bergemann, C., 2001. Clinical applications of magnetic drug targeting. J. Surg. Res. 95 (2), 200–206. https://doi.org/10.1006/jsre.2000.6030.

Manzoori, A., Fallah, F., Sharzehee, M., Ebrahimi, S., n.d. Computational investigation of the stability of stenotic carotid artery under pulsatile blood flow using a fluid-structure interaction approach. Int. J. Appl. Mech. 0, null. 10.1142/S1758825120501100.

Marín, T., Montoya, P., Arnache, O., Pinal, R., Calderón, J., 2018. Development of magnetite nanoparticles/gelatin composite films for triggering drug release by an external magnetic field. Mater. Des. 152, 78–87. https://doi.org/10.1016/j.matdes.2018.04.073.

Nilsestuen, J.O., Hargett, K.D., 2005. Using ventilator graphics to identify patient-ventilator asynchrony. Respir. Care 50, 202–232.

Nowak, N., Kakade, P.P., Annapragada, A.V., 2003. Computational fluid dynamics simulation of airflow and aerosol deposition in human lungs. Ann. Biomed. Eng. 31 (4), 374–390. https://doi.org/10.1114/1.1560632.

Ostrovski, Y., Dorfman, S., Mezhericher, M., Kassinos, S., Sznitman, J., 2019. Targeted drug delivery to upper airways using a pulsed aerosol bolus and inhaled volume tracking method. Flow. Turbul. Combust. 102 (1), 73–87. https://doi.org/10.1007/s10494-018-9927-1.

Ostrovski, Y., Dorfman, S., Poh, W., Chye Joachim Loo, S., Sznitman, J., 2021. Focused targeting of inhaled magnetic aerosols in reconstructed in vitro airway models. J. Biomech. 118, 110279. https://doi.org/10.1016/j.jbiomech.2021.110279.

Ostrovski, Y., Hofemeier, P., Sznitman, J., 2016. Augmenting regional and targeted delivery in the pulmonary acinus using magnetic particles. Int. J. Nanomed. 11 https://doi.org/10.2147/IJN.S102138.

Patwa, A., Shah, A., 2015. Anatomy and physiology of respiratory system relevant to anaesthesia. Indian J. Anaesth. https://doi.org/10.4103/0019-5049.165849.

Poh, W., Ab Rahman, N., Ostrovski, Y., Sznitman, J., Pethe, K., Loo, S.C.J., 2019. Active pulmonary targeting against tuberculosis (TB) via triple-encapsulation of Q203, bedaquiline and superparamagnetic iron oxides (SPIOs) in nanoparticle aggregates. Drug Deliv. 26 (1), 1039–1048. https://doi.org/10.1080/10717544.2019.1676841.

Price, D.N., Stromberg, L.R., Kunda, N.K., Muttil, P., 2017. In vivo pulmonary delivery and magnetic-targeting of dry powder nano-in-microparticles. Mol. Pharm. 14 (12), 4741–4750. https://doi.org/10.1021/acs.molpharmaceut.7b0053210.1021/acs.molpharmaceut.7b00532.s001.

Saadat, M., Manshadi, M.K.D., Mohammadi, M., Zare, M.J., Zarei, M., Kamali, R., Sanati-Nezhad, A., 2020. Magnetic particle targeting for diagnosis and therapy of lung cancers. J. Control. Release 328, 776–791. https://doi.org/10.1016/j.jconrel.2020.09.017.

Sabz, M., Kamali, R., Ahmadizade, S., 2019. Numerical simulation of magnetic drug targeting to a tumor in the simplified model of the human lung. Comput. Methods Programs Biomed. 172, 11–24. https://doi.org/10.1016/j.cmpb.2019.02.001.

Shamloo, A., Amani, A., Forouzandehmehr, M., Ghoytasi, I., 2019. In Silico study of patient-specific magnetic drug targeting for a coronary LAD atherosclerotic plaque. Int. J. Pharm. 559, 113–129. https://doi.org/10.1016/j.ijpharm.2018.12.088.

Shamloo, A., Ebrahimi, S., Amani, A., Fallah, F., 2020. Targeted drug delivery of microbubble to arrest abdominal aortic aneurysm development: a simulation study towards optimized microbubble design. Sci. Rep. https://doi.org/10.1038/s41598-020-62410-3.

Shamloo, A., Forouzandehmehr, M., 2019. Personalised deposition maps for micro- and nanoparticles targeting an atherosclerotic plaque: attributions to the receptor-mediated adsorption on the inflamed endothelial cells. Biomech. Model. Mechanobiol. 18 (3), 813–828. https://doi.org/10.1007/s10237-018-01116-y.

Shamloo, A., Mohammadaliha, N., Mohseni, M., 2015a. Integrative utilization of microenvironments, biomaterials and computational techniques for advanced tissue engineering. In. J. Biotech. 212, 71–89. https://doi.org/10.1016/j.jbiotec.2015.08.005.

Shamloo, A., Pedram, M.Z., Heidari, H., Alasty, A., 2016. Computing the blood brain barrier (BBB) diffusion coefficient: a molecular dynamics approach. J. Mag. Mag. Mat. 410, 187–197. https://doi.org/10.1016/j.jmmm.2016.03.030.

Shamloo, A., Manuchehrfar, V., Rafii-Tabar, H., 2015b. A viscoelastic model for axonal microtubule rupture. J. Biomech. 48 (7), 1241–1247.

Shamloo, A., Nejad, M.A., Saeedi, M., 2017. Fluid–structure interaction simulation of a cerebral aneurysm: effects of endovascular coiling treatment and aneurysm wall thickening. J. Mech. Behav. Biomed. Mat. 74.

Sirsi, S.R., Fung, C., Garg, S., Tianning, M.Y., Mountford, P.A., Borden, M.A., 2013. Lung surfactant microbubbles increase lipophilic drug payload for ultrasound-targeted delivery. Theranostics 3 (6), 409–419. https://doi.org/10.7150/thno.5616.

Sohrabi, S., Zheng, J., Finol, E.A., Liu, Y., 2014. Numerical simulation of particle transport and deposition in the pulmonary vasculature. J. Biomech. Eng. DOI 10 (1115/1), 4028800.

Sun, C., Lee, J.S.H., Zhang, M., 2008. Magnetic nanoparticles in MR imaging and drug delivery. Adv. Drug Deliv. Rev. 60 (11), 1252–1265. https://doi.org/10.1016/j.addr.2008.03.018.

Ta, H.T., Truong, N.P., Whittaker, A.K., Davis, T.P., Peter, K., 2018. The effects of particle size, shape, density and flow characteristics on particle margination to vascular walls in cardiovascular diseases. Expert Opin. Drug Deliv. 15 (1), 33–45. https://doi.org/10.1080/17425247.2017.1316262.

Tan, J., Wang, S., Yang, J., Liu, Y., 2013. Coupled particulate and continuum model for nanoparticle targeted delivery. Comput. Struct. 122, 128–134. https://doi.org/10.1016/j.compstruc.2012.12.019.

Tom, R.T., Suryanarayanan, V., Reddy, P.G., Baskaran, S., Pradeep, T., 2004. Ciprofloxacin-protected gold nanoparticles. Langmuir 20 (5), 1909–1914. https://doi.org/10.1021/la035856710.1021/la0358567.s001.

Toth, A., Kelley, C.T., Slattery, S., Hamilton, S., Clarno, K., Pawlowski, R., 2015. Analysis of anderson acceleration on a simplified neutronics/thermal hydraulics system, in: Mathematics and Computations, Supercomputing in Nuclear Applications and Monte Carlo International Conference, M and C+SNA+MC 2015.

Toy, R., Hayden, E., Shoup, C., Baskaran, H., Karathanasis, E., 2011. The effects of particle size, density and shape on margination of nanoparticles in microcirculation. Nanotechnology 22. https://doi.org/10.1088/0957-4484/22/11/115101.

Tzotzos, S.J., Fischer, B., Fischer, H., Zeitlinger, M., 2020. Incidence of ARDS and outcomes in hospitalized patients with COVID-19: a global literature survey. Crit. Care. https://doi.org/10.1186/s13054-020-03240-7.

Umbarkar, T.S., Kleinstreuer, C., 2015. Computationally efficient fluid-particle dynamics simulations of arterial systems. Commun. Comput. Phys. 17 https://doi.org/10.4208/cicp.160114.120914a.

Urbina, M.C., Zinoveva, S., Miller, T., Sabliov, C.M., Monroe, W.T., Kumar, C.S.S.R., 2008. Investigation of magnetic nanoparticle-polymer composites for multiple-controlled drug delivery. J. Phys. Chem. C 112. https://doi.org/10.1021/jp711517d.

Verma, N.K., Crosbie-Staunton, K., Satti, A., Gallagher, S., Ryan, K.B., Doody, T., McAtamney, C., MacLoughlin, R., Galvin, P., Burke, C.S., Volkov, Y., Gun'ko, Y.K., 2013. Magnetic core-shell nanoparticles for drug delivery by nebulization. J. Nanobiotechnol. 11 https://doi.org/10.1186/1477-3155-11-1.

Widder, K.J., Senyei, A.E., Scarpelli, D.G., 1978. Magnetic microspheres: a model system for site specific drug delivery in vivo. Proc. Soc. Exp. Biol. Med. 158 https://doi.org/10.3181/00379727-158-40158.

Xu, H., Song, T., Bao, X., Hu, L., 2005. Site-directed research of magnetic nanoparticles in magnetic drug targeting, in. J. Magn. Magn. Mater. https://doi.org/10.1016/j.jmmm.2005.01.067.

Zhou, Z., Price, C.C., 2020. Overview on the use of IL-6 agents in the treatment of patients with cytokine release syndrome (CRS) and pneumonitis related to COVID-19 disease. Expert Opin. Investig. Drugs. https://doi.org/10.1080/13543784.2020.1840549.